Supporting Information for: Kβ Mainline X-ray Emission Spectroscopy as an Experimental Probe of Metal-Ligand Covalency

Christopher J. Pollock,[a†] Mario Ulises Delgado-Jaime,[a] Mihail Atanasov,[a,c] Frank Neese, [a]* Serena DeBeer[a,b]**

[a] Max-Planck-Institut für Chemische Energiekonversion, Mülheim an der Ruhr, D-45470 Germany

[b] Department of Chemistry and Chemical Biology, Cornell University, Ithaca, NY 14853, United States

[c] Institute of General and Inorganic Chemistry, Bulgarian Academy of Sciences, 1113 Sofia, Bulgaria

[†] Current Address: Department of Chemistry, The Pennsylvania State University, University Park, PA 16802, United States

serena.debeer@cec.mpg.de

mihail.atanasov@cec.mpg.de

frank.neese@cec.mpg.de

1 Sample ORCA Geometry Optimization Input File

```
! UKS BP86 def2-TZVP def2-TZV/J TightSCF SlowConv SCFConv7 COSMO ZORA
! Grid4 NoFinalGrid Normalprint
! OPT
! PAL2

%scf
      MaxIter 500
      end

%maxcore 1024

%method SpecialGridAtoms 26
         SpecialGridIntAcc 7
         end

* xyzfile -3 6 FeF6.xyz
```

2 Sample ORCA Calculation to Generate QROs

```
! UKS BP86 def2-TZVP def2-TZV/J TightSCF SlowConv SCFConv7 COSMO ZORA UNO
! Grid4 NoFinalGrid Normalprint

%scf
      MaxIter 500
      end

%maxcore 1024

%method SpecialGridAtoms 26
         SpecialGridIntAcc 7
         end

* xyzfile -3 6 FeF6_opt.xyz
```

3 Sample CASSCF Calculation Input File

```
! def2-TZVP def2-TZV/J COSMO ZORA VeryTightSCF
! Grid4 NoFinalGrid Normalprint
! MOREAD
! PAL4

%moinp"FeF6_orbs.qro"

%scf
      MaxDisk 400000
      rotate {22,34,90} {23,35,90} {27,36,90} {28,37,90} {29,38,90} end
end

%casscf
      nel 15
      norb 10
      mult 6,4,2
      nroots 1,24,75
      bweight = 1,1,1
      trafostep RI
      maxiter 500
end

%method SpecialGridAtoms 26
         SpecialGridIntAcc 7
         end

* xyzfile -3 6 FeF6_opt.xyz
```

4 Sample RAS-CI Calculation Input File

```
! RHF AllowRHF def2-TZVP def2-TZV/J COSMO ZORA
! NormalPrint
! MOREAD NOITER
! NoLoewdin NoMulliken

%moinp "FeF6_orbs.qro"

%scf
  MaxDisk 400000
  rotate {0,35,90} {12,36,90} {13,37,90} {14,38,90} end
end

%basis gtoaux autobuild
 end

%mrci citype mrci
  UseIVOs false
  Etol 1e-5
  IntMode ritrafo
  newblock 7 *
    excitations none
    nroots 4
    refs ras(12:4 1/5/0 0) end
    end
  newblock 5 *
    excitations none
    nroots 105
    refs ras(12:4 1/5/0 0) end
    end
  soc
  dosoc true
  NInitstates 500
  end
end

%method SpecialGridAtoms 26
         SpecialGridIntAcc 7
         end

* xyzfile -2 5 FeF6_opt.xyz
```

5 Sample Crystal Field Multiplet Input File (.rcg)

```
   10    1    0   14    2    4    1    1 SHELL03000000 SPIN03000000 INTER8
    0                         80998070            8065.47800     0000000
    1     3 1 13 1 10          00      9 00000000 0 8065.4790 .00       1
S 1  D 5  P 6
S 2  D 5  P 5
Fe3+ 1S01 3D05     5    0.0000   13.7111    8.6181    0.0842    0.0000HR99999999
Fe3+ 3P05 3D05     8    0.0000   13.0391    8.2021    0.0662    1.0032HR99999999
   13.7173   16.9124   10.3884
Fe3+ 1S01 3D05      Fe3+ 3P05 3D05         0.01362( 3P//R1// 1S) 0.957HR  14 -99
                    -99999999.
   -1
```

Several of the parameters contained in this file are relevant to the current study. The reductions to the atomic parameters can be found in the "80998070" block located on the second line of code. The first two digits (80) control the reduction of the F_{dd} parameters, the second two (99) govern the spin-orbit coupling constants, while the remaining "80" and "70" reduce the F_{pd} and G_{pd} parameters, respectively.

The next relevant inputs are found on lines 4 and 5 (e.g. "S 1 D 5 P 6") and these govern the configurations used for the initial and final states of the calculation. As defined here, the initial state has a single s electron, five d electrons, and a filled p shell while the final state has a filled s orbital and a hole in the p shell.

Lastly, the actual values of the atomic parameters used in the calculation are found on lines 6 – 8. Explicitly, for the initial state the "13.711" and "8.618" are the F_{dd}^2 and F_{dd}^4 values, respectively—note that the final "1" present for each of these is not a digit of the parameter but rather a code specifying the number as a F_{dd} parameter—and the "0.084" defines the ζ_{3d} spin-orbit coupling (again, the final "2" is not a digit but a code indicating spin-orbit coupling). Analogous parameters are found for the final state, with the trailing "3" specifying a F_{pd} integral and "4"s defining the G_{pd} parameters. While these values can be manually edited, it is highly recommended to use the block on the second line instead.

Additional detail and further explanations for this input file can be found at:

http://www.anorg.chem.uu.nl/people/staff/FrankdeGroot/XAFSdata/MANOO/Mrcn1.htm

6 Sample Crystal Field Multiplet Input File (.rac)

```
Y

    % vertical 1 1

 butler O3

 to    Oh

 to    D4h

 to    C4h

 endchain

 actor   0+ HAMILTONIAN ground  PRINTEIG

  OPER HAMILTONIAN

    BRANCH 0+ > 0 0+ > 0+    > 0+   1.0

  OPER SHELL2

    BRANCH 4+ > 0 0+ > 0+    > 0+   3.286
    BRANCH 4+ > 0 2+ > 0+    > 0+   0.000
    BRANCH 2+ > 0 2+ > 0+    > 0+   0.000
  OPER SPIN2

    BRANCH 1+ > 0 1+ > ^0+   > 0+   0.000
  OPER ORBIT2

    BRANCH 1+ > 0 1+ > ^0+   > 0+   0.000
 actor   0+ HAMILTONIAN excite  PRINTEIG

  OPER HAMILTONIAN

    BRANCH 0+ > 0 0+ > 0+    > 0+   1.0

  OPER SHELL2

    BRANCH 4+ > 0 0+ > 0+    > 0+   3.286
    BRANCH 4+ > 0 2+ > 0+    > 0+   0.000
    BRANCH 2+ > 0 2+ > 0+    > 0+   0.000
  OPER SPIN2

    BRANCH 1+ > 0 1+ > ^0+   > 0+   0.000
  OPER ORBIT2

    BRANCH 1+ > 0 1+ > ^0+   > 0+   0.000
 actor   1- left        transi PRINTTRANS

   oper MULTIPOLE

     branch  1- > 0 1- >  1- >  1-  1.000
```

```
 actor  -1- right       transi PRINTTRANS

   oper MULTIPOLE

     branch  1- > 0 1- >  1- > -1-  1.000

 actor   0- parallel    transi PRINTTRANS

   oper MULTIPOLE

     branch  1- > 0 1- > ^0- >  0-  1.000

RUN
```

This .rac file contains the information needed to control the imposition of a crystal field in the multiplet calculations. The value "`3.286`" found on lines 23 and 40 indicates an octahedral crystal field of 1.0 eV and can be modified to achieve any field strength. Due to unit conversions, the desired crystal field in electron volts must be multiplied by a factor of 3.286 for use in this input file (e.g. a field of 1.5 eV would need a value of 4.929).

7 Python Script Used to Extract RAS-CI Transitions from ORCA Outputs

```
#!/usr/bin/env python
# Dimitrios G. Liakos
#Usage: SelectedTransitions.py  ORCAFilename   LowInitialState    HighInitialState
LowFinalState  HighFinalState

import os
import re
import string
import fileinput
from optparse import OptionParser

parser              = OptionParser()
(options, args ) = parser.parse_args()

ORCAFilename = args[0]
SelectedFilename = "SelectedFile.out"
IS     = int(args[1])
IE     = int(args[2])
FS     = int(args[3])
FE     = int(args[4])
AI     = -999
AF     = -999
SRead  = re.compile("SPIN-ORBIT CORRECTED MRCI ABSORPTION SPECTRUM")
SReadLine = -999
EndReading    = re.compile("SOC STATE DIPOLE MOMENTS")
EReadLine     = -999

CurrentDirectory = os.path.abspath("./")
AbsORCAFilename = os.path.join(CurrentDirectory, ORCAFilename)
AbsSelectedFilename = os.path.join(CurrentDirectory, SelectedFilename)
Info = open(AbsSelectedFilename, 'wb')

for line in fileinput.input(AbsORCAFilename):
       if SRead.search(line) != None:
              SReadLine = fileinput.lineno() + 5
       if EndReading.search(line) != None and SReadLine > 0:
              EReadLine     = fileinput.lineno() - 3
              break
fileinput.close()
for line in fileinput.input(AbsORCAFilename):
       if fileinput.lineno() >= SReadLine and fileinput.lineno() <= EReadLine :
              parts = string.split(line)
              AI     = int(parts[0])
              AF     = int(parts[1])
              if AI >= IS and AI <= IE :
                     if AF >= FS and AF <= FE :
                            Info.write(line)

fileinput.close()
Info.close
```

Assuming the script is saved as SelectedTransitions3.py, the syntax to run it is as follows:

```
C:\python32\python SelectedTransitions3.py ORCAoutput.out X Y A B
```

Where X = # of lowest energy intermediate state, Y = highest energy intermediate state, A = lowest energy final state, B = highest energy final state.

8 Representative Mainline Fits for All Compounds

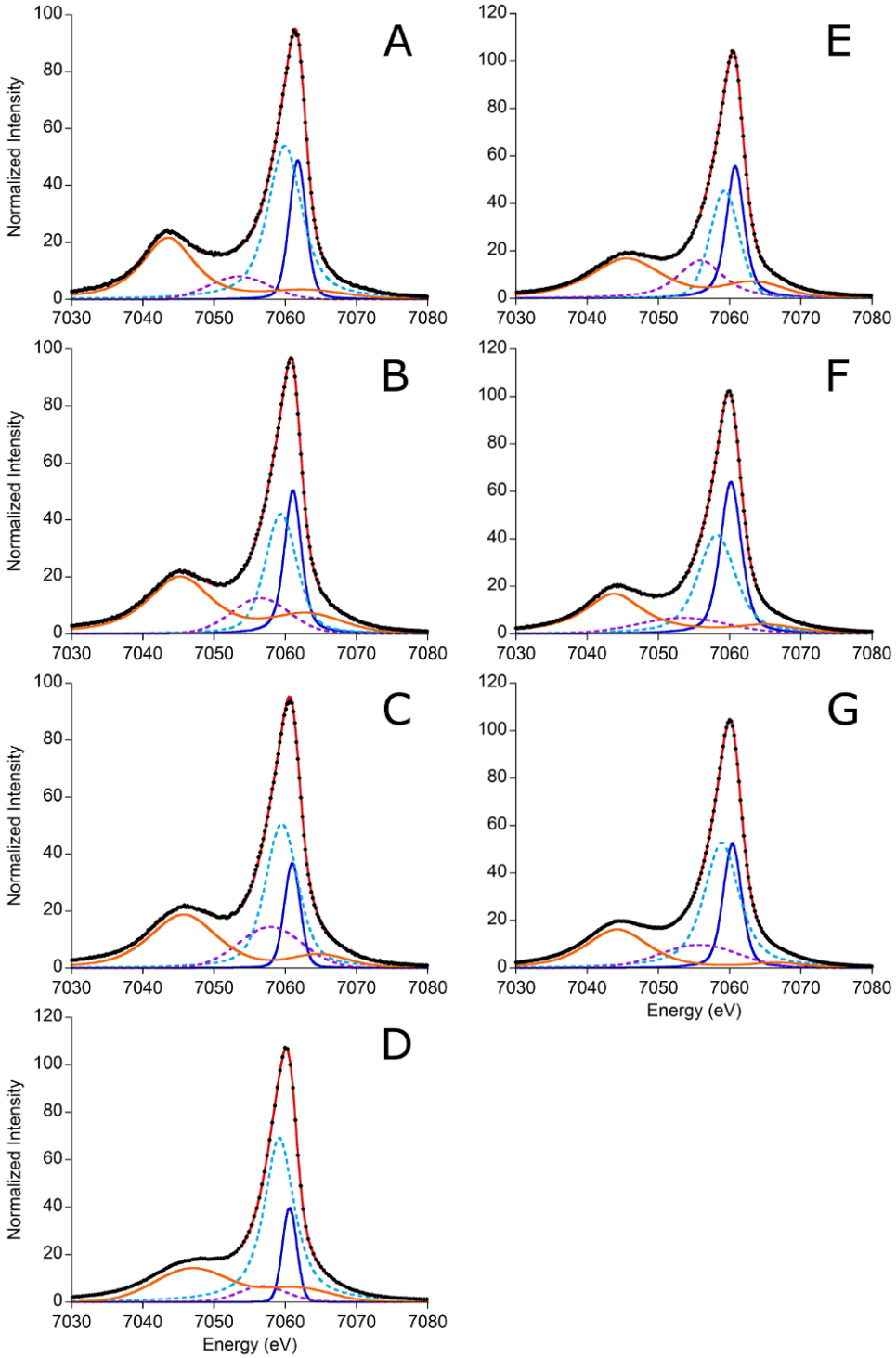

Figure S1: Representative mainline fits for all compounds (A = FeF_3; B = $FeCl_3$; C = $FeBr_3$; D = $Fe(SAr)_4^{1-}$; E = $FeCl_4^{1-}$; F = $Fe(acac)_3$; G = (tpfp)FeCl). A total of five fit components were required to satisfactorily reproduce the data in these spectra; for technical reasons, two of these fit peaks were plotted together as the orange component. The position of the low energy orange and high energy blue fit components were used for determination of ΔE as found in Table 1.

9 Explanation of Crystal Field Multiplet Calculations

Crystal field multiplet calculations have been the standard method for simulation of Kβ mainline spectra for many years and often have excellent agreement with experiment. Despite the extensive work already done in this area, we undertake a systematic investigation of d^5 Fe(III) systems here so as to better correlate our new RAS-CI approach to what has previously been done.

As mentioned in the main text, various parameters can be adjusted to modify spectral shape. In the following figures we demonstrate that parameters other than G_{pd} have very limited impact on spectral shape, thus reductions of G_1 and G_3 alone are sufficient to reproduce the experimentally observed splittings. We begin first with the spin-orbit coupling constants, ζ_{3p} and ζ_{3d} (Figure S2). Inclusion of spin-orbit coupling further splits the observed multiplets, though within the experimental resolution it has negligible effect on the spectral shape. Given the small value of 3d spin-orbit coupling (<0.1 eV), this result is perhaps not surprising.

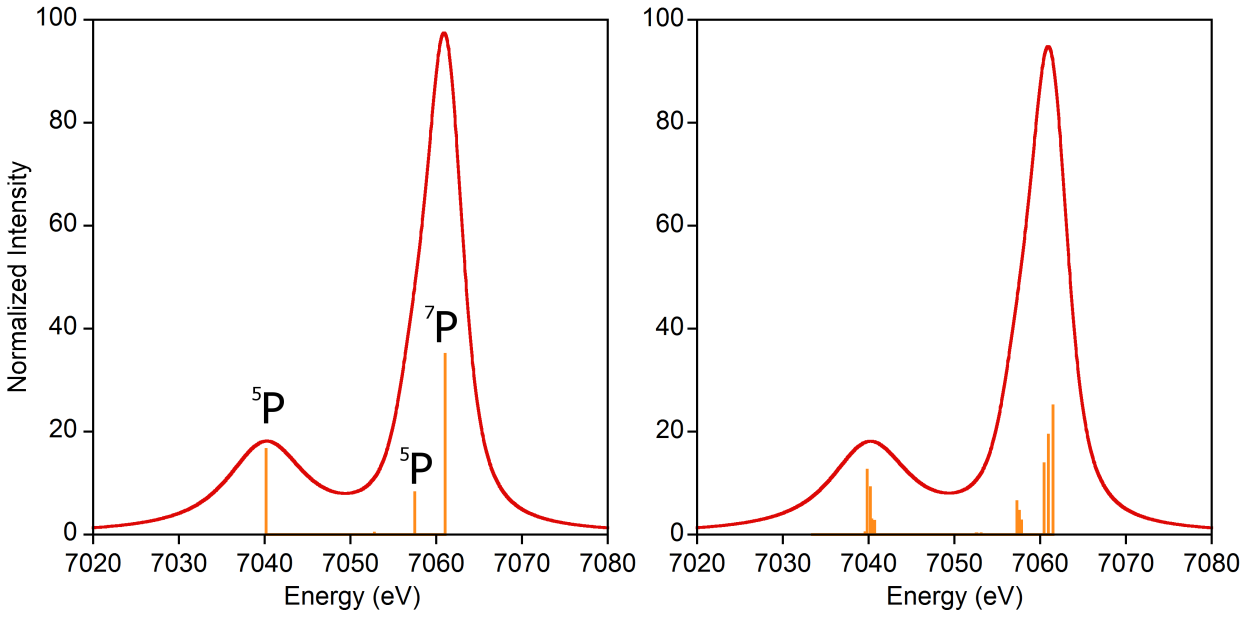

Figure S2: Kβ XES mainlines calculated with Slater integrals set to 80% of their calculated values, no crystal field, and no spin orbit coupling (left) or with spin orbit coupling set to 100% of its calculated value (right). With the level of broadening employed (1.6 / 5.1 eV), the spectral shapes are nearly identical. A small feature at ~7053 eV is present, but too low in intensity to be visible.

Modifying either of the repulsion parameters, F_{dd} and F_{pd}, resulted in relatively small changes in the calculated mainline spectra. Reducing F_{dd} had the effect of compressing the spread of transition energies of the final states, thus providing a ΔE that is reduced by 1.6 eV across the series. Reducing F_{pd} has the opposite effect and serves to increase the splitting among the final states by 1 eV across the series. However, unrealistically large reductions in the electron-electron repulsion parameters (>90% reductions) are necessary to achieve these effects (Figure S3); modifications within chemically realistic regimes necessarily would produce much smaller changes in the observed splitting and are unable to account for the experimental observations.

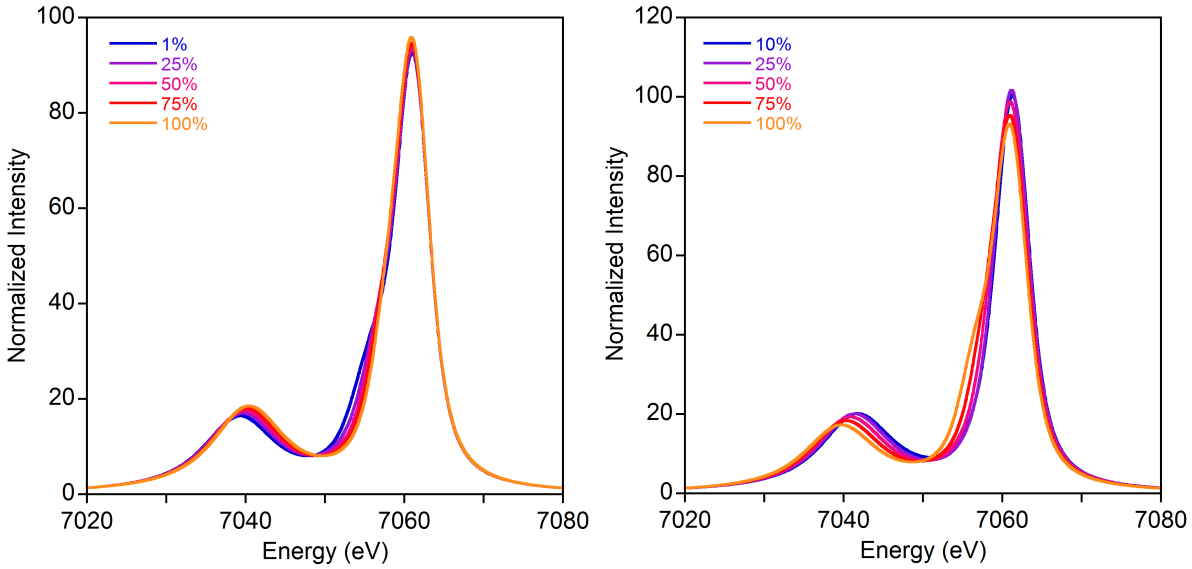

Figure S3: Plots showing that the effects of F_{pd} (left) and F_{dd} (right) are minimal within chemically-relevant values.

Variation of the crystal field splitting from the free ion limit to a very large value of 3 eV also yielded negligible changes to the calculated spectra (Figure S4). Further increases induce a change from a high spin to a low spin ground state and thus are not shown.

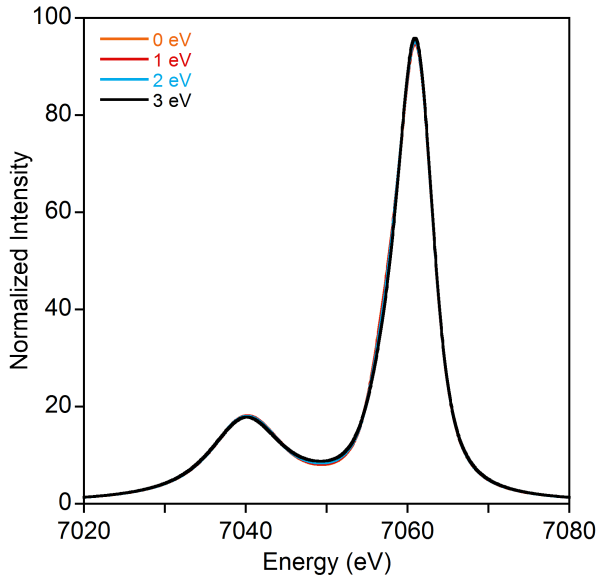

Figure S4: Spectra calculated using a crystal field multiplet approach that vary only in the magnitude of 10 Dq.

From the observation, explored in the main text, that the p-d exchange integral exerts almost exclusive control over the Kβ' – $K\beta_{1,3}$ splitting, we attempted to reproduce the experimental spectra of this series by reducing the G_{pd} values. Via these reductions, agreement with the experimentally observed splitting could be achieved (Figure S5), with the amount of reduction required in acceptable agreement with the coefficients from the QROs. Deviations from

experiment could likely be reduced by the inclusion of charge transfer effects, which were not investigated here. By performing fits with fixed values of F_{pd} and F_{dd} so as to minimize or maximize the mainline splitting, we estimate the uncertainty associated with the obtained G_{pd} reductions to be approximately ±5%.

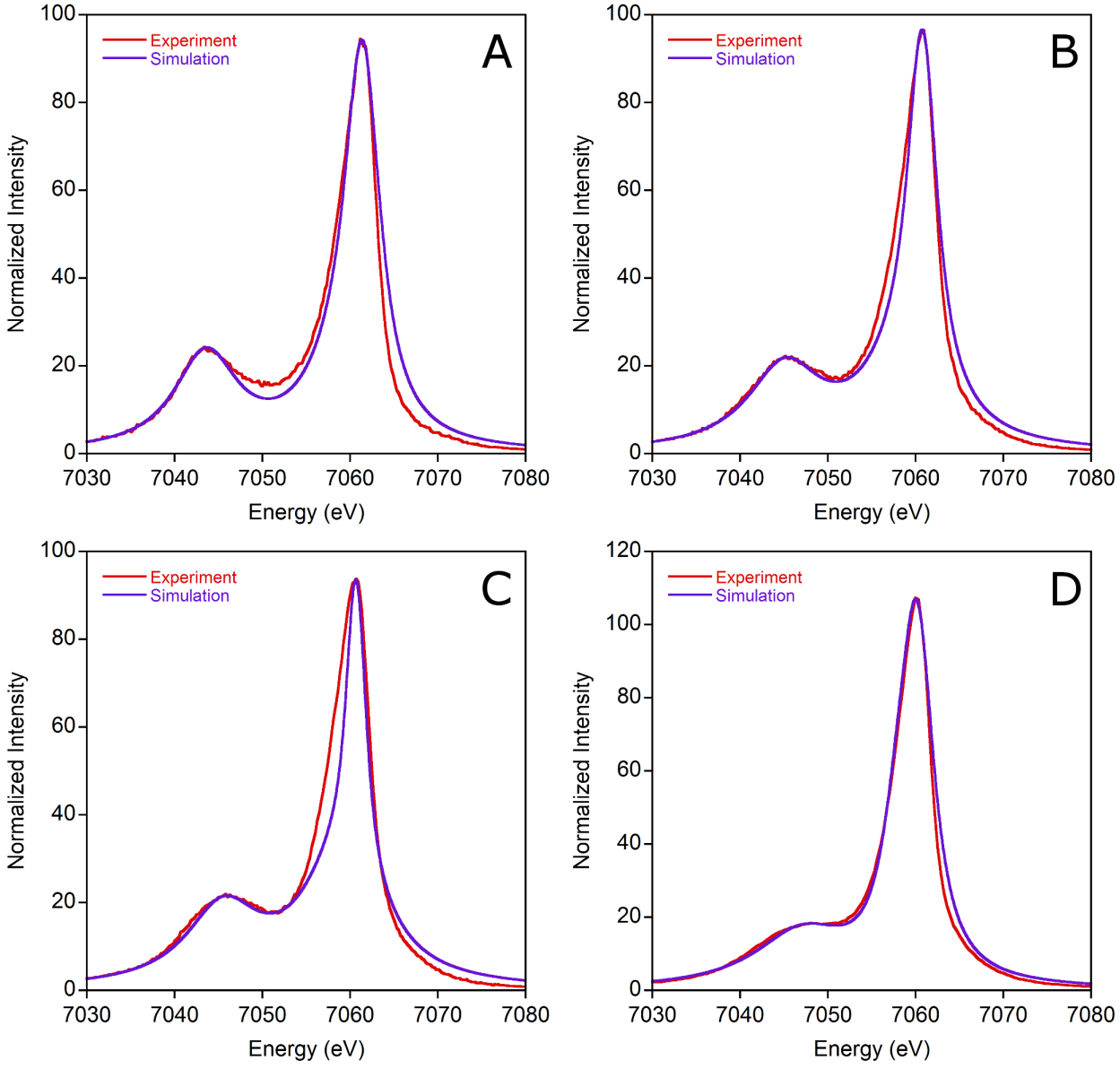

Figure S5: Mainlines simulations using multiplet calculations (A = FeF_3, B = $FeCl_3$, C = $FeBr_3$, D = $Fe(SAr)_4^{1-}$).

Table S1: Numerical parameters for mainline simulations

	Slater Reduction*
FeF_3	68%
$FeCl_3$	59%
$FeBr_3$	56%
$Fe(SAr)_4^{1-}$	50%

* The reductions reported here are reductions applied to the Hartree-Fock values that are used in the program. Because the Hartree-Fock methodology overestimates these integrals, a reduction to 80% of the calculation is necessary to obtain the correct "atomic" values as obtained by atomic spectroscopy; thus, a reported reduction of 68% correlates to an 85% reduction from the atomic value (0.68 / 0.8). Further discussion on this topic can be found in work from de Groot and coworkers.[1] Spin orbit coupling was maintained at 100% of the tabulated value in all calculations.

10 Explanation of RAS-CI Inputs

As mentioned in the main text, the RAS-CI calculations undertaken here calculate the transitions between $1s^1 3p^6 3d^5$ and $1s^2 3p^5 3d^5$ states. The starting orbitals (QROs) are input from a DFT calculation and are kept frozen for the RAS-CI calculations. In these calculations the 1s and 3p orbitals are first rotated to the positions right below the partially occupied d-shell. An electron is then removed from the system and a RAS(12: 4 1/ 5 / 0 0) calculation is performed for multiplicities 5 and 7, consistent with the qualitative discussion given in the introduction. Here the notation RAS(n_{el}: m_1 n_1/ m_2 / m_3 n_3) stands for a restricted active space with a total of n_{el} electrons, up to n_1 holes in m_1 orbitals (RAS1 space) and up to n_3 particles (electrons) in m_3 orbitals (RAS3 space) while m_2 orbitals can carry any number of holes or particles (RAS2 space). Thus, the notation above implies twelve electrons in the CI calculation (five 3d-electrons, six 3p-electrons and one 1s electron). Configurations are constructed such that the 1s and 3p shells together can carry at most one hole (thus covering the $1s^2 3p^6 3d^4$ $1s^1 3p^6 3d^5$ and $1s^2 3p^5 3d^5$ configurations, m_1=4) while any occupation is allowed in the d-orbitals (m_2=5) and no excitation is performed from any of doubly occupied ligand orbitals nor into any of the empty virtual orbitals.

For each spatial configuration all linearly independent configuration state functions (CSFs) are constructed. The so obtained "non-relativistic" roots are allowed to interact via the SOC operator, which in ORCA is represented by the spin-orbit mean-field (SOMF) operator as described in ref 2. Thus, the calculation takes care of all multiplet and SOC effects and incorporates metal-ligand covalency explicitly via the shapes and compositions of the orbitals. The SOMF operator is an effective, non-empirical one-particle operator but explicitly contains the spin-same-orbit and spin-other orbit interactions in its definition. To this end, one needs to generate all M_s sublevels of each multiplet of total spin S which is accomplished by using the Wigner-Eckart theorem as explained in detail in refs 2-4. Finally, transition moments are calculated between the various spin-orbit coupled many particle states. Care must be taken to include all possible $1s^1 3p^6 3d^5$ multiplets as initial (or intermediate after ionization) states in order to obtain a consistent emission spectral shape arising from all possible initial into all possible $1s^2 3p^5 3d^5$ final states (note carefully that what is referred to as "initial state" are the "intermediate" states referred to in Figure 2)

To motivate the number of roots calculated, we consider the accessible states from all three configurations that are involved in an XES experiment ($1s^1 3p^6 3d^5$, $1s^2 3p^5 3d^5$, $1s^2 3p^6 3d^4$). For example, there is one possible septet state for $1s^1 3p^6 3d^5$, three for $1s^2 3p^5 3d^5$, and none for $1s^2 3p^6 3d^4$, so the number of roots to calculate for the septets is four. Likewise, for the quintets there are 105 possible states [25 ($1s^1 3p^6 3d^5$) + 75 ($1s^2 3p^5 3d^5$) + 5 ($1s^2 3p^6 3d^4$)]. For Kβ mainlines, all $1s^2 3p^5 3d^5$ states are accessible; however, since states are necessarily calculated from lowest to highest energy, all lower-lying $1s^2 3p^6 3d^4$ multiplets must be included as well. Thus for a septet calculation all septets from $1s^2 3p^6 3d^4$ (zero) as well as from $1s^2 3p^5 3d^5$ (three) must be accounted for. This number must be multiplied by the multiplicity (7) since all M_s components are explicitly treated to yield a total of 3x7=21 "initial" states for the calculation of transition moments. For the quintets the same reasoning leads to 75 states from $1s^2 3p^5 3d^5$ plus five from $1s^2 3p^6 3d^4$ multiplied by a multiplicity of five to yield 400 "initial" states. Treating the septets and quintets simultaneously thus requires a minimum of at least 421 necessary initial states (a value of 500 was used in these calculations). This procedure can of course be

generalized for any d^n count metal ion, provided that the appropriate electronic configurations and multiplicities are selected as inputs for the computations.

The result of this calculation is a compilation of all possible transitions between all of the states; as most of this information is not relevant to the calculation of Kβ mainlines, the necessary transitions must be selected for plotting. Because Kβ mainlines correspond to 3p to 1s transitions, only transitions between these states are needed. Furthermore, it is expected that only the lowest energy $1s^1 3p^6 3d^5$ state will initially be populated. Thus, ultimately only transitions between the $1s^2 3p^5 3d^5$ derived states and the lowest energy $1s^1 3p^6 3d^5$ states need to be selected. Selection of only these transitions was accomplished by means of a Python script. Sample input files for all of these calculations and the required Python script are found above.

Lastly, rather than using QROs, orbitals for input into RAS-CI calculations can also be generating from a complete active space self-consistent field (CASSCF) calculation. In the CASSCF calculations, an average over the unique sextet, the 24 quartet, and 75 doublet states is performed; thus, the present calculations can also be interpreted as configuration averaged Hartree-Fock calculations.Regardless of whether QROs or CASSCF orbitals are employed, the RAS-CI procedure remains unchanged.

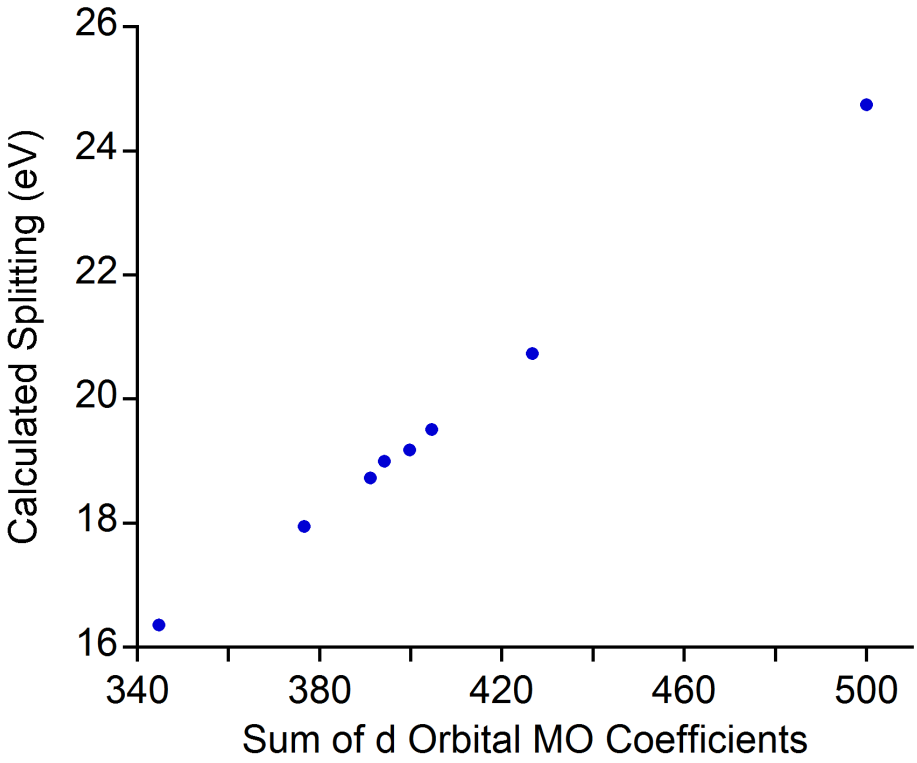

Figure S6: Correlation between the ΔE obtained from RAS-CI calculations and QRO coefficients on the metal-based d orbitals as given in Table 3.

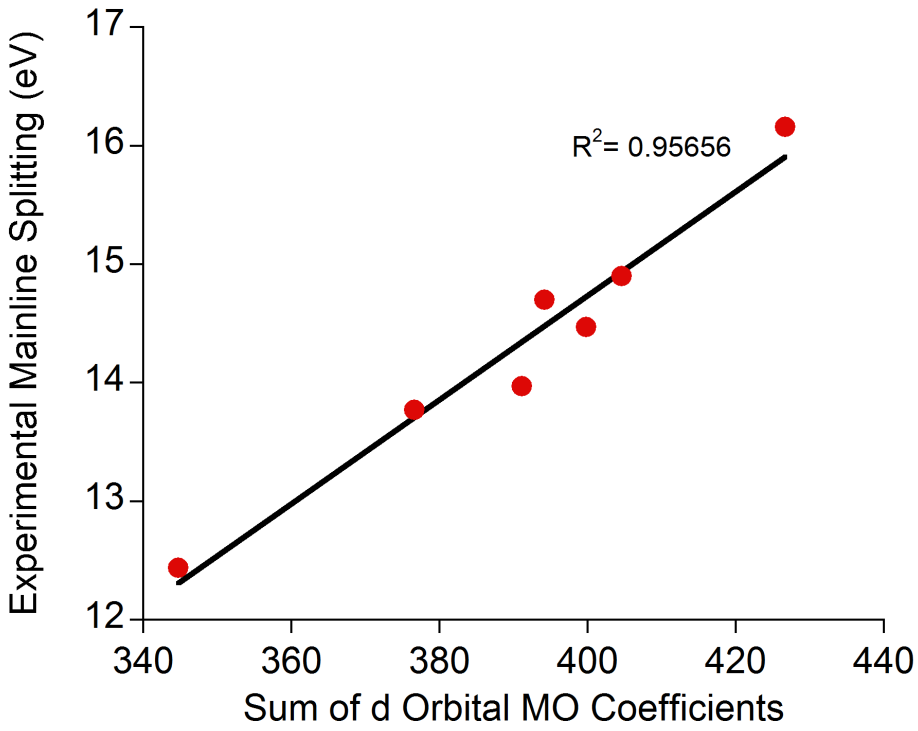

Figure S7: The correlation between the QRO coefficients on the metal-based d orbitals and the mainline splitting as determined from the intensity-weighted average energies of the Kβ' and $K\beta_{1,3}$ peaks. Thus, the trend observed in Figure 10 holds regardless of how the experimental mainline splitting is measured.

Table S2: Numerical parameters for mainline fits

	Kβ' Position*	$K\beta_{1,3}$ Position (fit peak)	$K\beta_{1,3}$ Position (IWAE)	ΔE (fit peak)	ΔE (IWAE)
FeF_3	7043.56	7061.73	7059.72	18.17	16.16
$FeCl_3$	7045.25	7061.06	7059.72	15.81	14.47
$FeBr_3$	7045.7	7060.97	7059.67	15.27	13.97
$Fe(SAr)_4^{1-}$	7046.97	7060.60	7059.41	13.63	12.44
$FeCl_4^{1-}$	7045.54	7060.78	7059.31	15.24	13.77
$Fe(acac)_3$	7043.75	7060.18	7058.65	16.43	14.90
(tpfp)FeCl	7044.21	7060.39	7058.91	16.18	14.70

* Because the Kβ' feature is composed of a single fit peak, the intensity-weighted average energy and fit peak position are the same.

11 Derivation of Analytic Equations for ΔE Dependence on the Metal Spin Ground State and Metal-Ligand Covalency Reduction Factors t and e.

Restricting the exchange coupling to that between 3p and 3d spins, the spin-dependent part of the energy has been computed using Dirac's exchange operator:

$$\hat{H}_{exc} = -\sum_{i\in p,j\in d} J_{ij}\hat{S}_i\hat{S}_j = -\sum_{i\in p,j\in d} K_{ij}(\hat{P}_{ij} - 1/2) \qquad \text{(SI-1)}$$

with K_{ij} being the parameter for the energy of exchange coupling (the exchange integral) between two spins in p and d orbitals (i and j, respectively) and $\hat{P}_{ij}$ being the operator exchanging spins but leaving the orbital part of the wavefunctions unaltered. The parameters K_{ij} have been parameterized following Slater-Condon theory of atomic structure times the Stevens covalent reduction factors (e and t) pertaining to 3d molecular orbitals of $\sigma(e_g)$ and $\pi(t_{2g})$ type (in octahedral symmetry). The operator of eq. SI-1 has been applied to spin-eigenfunctions built up of linear combinations of 3p and 3d products of spin-uncoupled orbital-dependent spin functions of S_p=1/2 (for 3p) and S_d=1/2 (d^1, d^9, low-spin d^5), 1 (d^2, d^8), 3/2 (d^3), 2 (high-spin d^4 and d^6) 5/2 (high-spin d^5) listed in Appendix 6 in the book by Olivier Kahn, Molecular Magnetism, Wiley-VCH, 1993, p-367-373. To eliminate complications due to orbitally degenerate levels (in the general case they can lead to an interesting orbitally dependent anisotropic exchange Hamiltonian), proper averaging over all three degenerate sublevels of $^2T_{1u}$(for 3p) and (in the case of a manifold of orbitally degenerate multiplet levels due to the d^n configuration of the 3d-metal) over the possible components of the irreducible representations of the octahedral point group for the respective electronic terms. Geometric or vibronic perturbations have been ignored. The resulting expressions are listed in Table S3.

Table S3. 3p-3d exchange integrals in dependence of symmetry of the involved 3d orbitals accounted for Stevens reduction factors t and e for t_2 and e orbitals, respectively.

$K(p_x,d_{xy})=(3G_1+24G_3)t^2$	$K(p_y,d_{xy})=(3G_1+24G_3)t^2$	$K(p_z,d_{xy})=15G_3t^2$
$K(p_x,d_{xz})= (3G_1+24G_3)t^2$	$K(p_y,d_{xz})=15G_3t^2$	$K(p_z,d_{xz})= (3G_1+24G_3)t^2$
$K(p_x,d_{yz})=15G_3t^2$	$K(p_y,d_{yz})=(3G_1+24G_3)t^2$	$K(p_z,d_{yz})= (3G_1+24G_3)t^2$
$K(p_x,d_{x2-y2})=(3G_1+24G_3)e^2$	$K(p_y,d_{x2-y2})=(3G_1+24G_3)e^2$	$K(p_z,d_{x2-y2})=15G_3e^2$
$K(p_x,d_{z2})=(G_1+18G_3)e^2$	$K(p_y,d_{z2})=(G_1+18G_3)e^2$	$K(p_z,d_{z2})= (4G_1+27G_3)e^2$

Taking as an example for the application of this formalism the coupling of a 3p-hole on a p_i orbital (i=x, y, z) with a single 3d-spin on the 3d –orbital dj (j=d_{xy}, d_{xz}, d_{yz}). Such a case pertains to final states of Kβ emission lines of d^1 free ions (Ti^{3+}, V^{4+}, Cr^{5+}). The two spins give rise to a single S=1 and S=0 coupled spin states of the 3p-3d pair described by the following two-electron wavefunctions:

$$\left|S=1,M_s=1\right\rangle = |\,\alpha_{pi}\alpha_{dj}\,| \tag{SI-2}$$

$$\left|S=0,M_s=0\right\rangle = (1/\sqrt{2})[|\,\alpha_{pi}\beta_{dj}\,| - |\,\beta_{pi}\alpha_{dj}\,|] \tag{SI-3}$$

Applying the exchange operator in the Dirac form (the second term of eq SI-1) and omitting the constant (1/2) term—it cancels when taking energy differences—we obtain:

$$\hat{H}_{exc}\left|S=1,M_s=1\right\rangle = |\,\alpha_{pi}\alpha_{dj}\,| \tag{SI-4}$$

$$\hat{H}_{exc}\left|S=0,M_s=0\right\rangle = (1/\sqrt{2})[|\,\beta_{pi}\alpha_{dj}\,| - |\,\alpha_{pi}\beta_{dj}\,|] = -\left|S=0,M_s=0\right\rangle \tag{SI-5}$$

We therefore obtain:

$$\left\langle S=1,M_s=1\right|\hat{H}_{exc}\left|S=1,M_s=1\right\rangle = -K_{ij} \tag{SI-6}$$

$$\left\langle S=0,M_s=0\right|\hat{H}_{exc}\left|S=0,M_s=0\right\rangle = K_{ij} \tag{SI-7}$$

and for the singlet splitting $\Delta E = E(S=0) - E(S=1) = J_{ij} = 2K_{ij}$ (SI-8)

Ignoring effects due to orbital degeneracy (Jahn-Teller coupling, spin-orbit coupling), we now average the exchange splitting energy ΔE over all possible combinations of the involved components of the orbitally degenerate states which, after substitution of the corresponding entries of Table S1, leads to:

$$\begin{aligned}\Delta E = -(2/9)[&K_{px,dxy}+K_{px,dxz}+K_{px,dyz}+K_{py,dxy}+K_{py,dxz}+K_{py,dyz}+K_{pzdxy}+K_{pz,dxz}+K_{pz,dyz}) = \\ -(2/9)[&(3G_1+24G_3)+(3G_1+24G_3)+(15G_3)+(3G_1+24G_3)+(15G_3)+(3G_1+24G_3)+ \\ &(15G_3)+(3G_1+24G_3)+(3G_1+24G_3)] = 4G_1+42G_3\end{aligned} \tag{SI-9}$$

Accounting for the covalent reduction due to the $^2T_2$ ground state of the d^1 ion by a factor t^2 we finally obtain:

$$\Delta E = (4G_1+42G_3)t^2 \tag{SI-10}$$

12 CI results for free atoms and ions

In order to substantiate the discussion in the paper, we further elaborate on the atomic CI results. Figure S8 shows variations of the theoretical Kβ emission spectral shape with the number of spins and with variations in the G_1(pd) and G_3(pd) exchange and F_2(pd) Coulomb integrals as one moves from one 3d metal in a given oxidation state to another. These calculations have been done using state average CASSCF wave functions, which were then employed in a non-relativistic RAS-CI run. Figure S8 demonstrates in a more detailed way the simple model used to arrive at Table 2 and Figure 4 of the main text. Here all multiplets are computed but only those giving non-zero intensity are included in Tables S4-S14 and the associated figures. For example, in Figure S9 it is shown how 3p-3d exchange for iso-electronic $3d^5$ ions increases with increasing charge. The increased nuclear charge renders the 3d and 3p functions more compact and hence intra atomic (Hund) exchange between the 3p-core hole and the 3d-open shell more efficient.

The set of Tables S4-S14 will allow the interested reader to correlate these atomic numbers with her or his measured Kβ mainline spectra and thus empirically, without recourse to any DFT/RAS-CI calculation, obtain experimental estimates of covalency. For example taking the experimental numbers in Table S4 and the CASSCF/RAS-CI energy for the splitting of the Kβ-line we obtain the following reductions factors: 18.17/24.77=0.73; 15.81/24.77=0.64; 15.27/24.77=0.62; 13.63/24.77=0.55, which, on average, compare well with the ones derived from QRO's: 0.85, 0.80, 0.78, 0.69. The correlation between these two sets of reduction factors allows one to make predictions possible for systems for which nothing is known prior to experiment.

Table S4. Non-relativistic up- and down- coupling of core hole spins with the d^n open shell multiplets in the initial ($1s^1 3d^n$) and final ($3p^5 3d^n$) states of the Kβ mainline x-ray emission and symmetry selection rules for Kβ mainline transitions in 3d-metal ions in dependence of the $3d^n$ configuration and the initial/final spin states.[a]

n (computed metal ions)	core ionizations		3d-ionization	selection rules dipole allowed transitions
	initial states ($1s^1 3d^n$)	final states ($3p^5 3d^n$)	d^{n-1}	
1 (Ti^{3+}, Cr^{5+}, Mn^{6+})	$^{1,3}D$	^{1}PDF ^{3}PDF	^{1}S	$^{1,3}D \rightarrow {}^{1,3}PDF$
2 (V^{3+}, Cr^{4+}, Mn^{5+}, Fe^{6+})	$^{2,4}F$	$^{2}SPDFGH$ (3 3 3 2) $^{4}SPDFG$ (2)	^{2}D	$^{2,4}F \rightarrow {}^{2,4}DFG$
3 (Cr^{3+}, Mn^{4+}, Fe^{5+})	$^{3,5}F$	$^{3}SPDFGHI$ (2 4 6 5 4 2) $^{5}SPDFG$ (2)	^{3}PF	$^{3,5}F \rightarrow {}^{3,5}DFG$
4 (Cr^{2+}, Mn^{3+}, Fe^{4+})	$^{4,6}D$	$^{4}SPDFGHI$ (2 4 6 5 4 2) ^{6}FDP	^{4}PF	$^{4,6}D \rightarrow {}^{4,6}PDF$
5 (Mn^{2+}, Fe^{3+})	$^{5,7}S$	$^{5}SPDFGH$ (3 3 3 2) ^{7}P	^{5}D	$^{5,7}S \rightarrow {}^{5,7}P$
6 (Fe^{2+}, Co^{3+})	$^{4,6}D$	$^{4}SPDFGHI$ (2 4 6 5 4 2) ^{6}FDP	$^{4}PDFG$ ^{6}S	$^{4,6}D \rightarrow {}^{4,6}PDF$
7 (Co^{2+}, Ni^{3+})	$^{3,5}F$	$^{3}SPDFGHI$ (2 4 6 5 4 2) $^{5}SPDFG$ (2)	$^{3}PDFGH$ (2 2) ^{5}D	$^{3,5}F \rightarrow {}^{3,5}DFG$
8 (Ni^{2+}, Cu^{3+})	$^{2,4}F$	$^{2}SPDFGH$ (3 3 3 2) $^{4}SPDFG$ (2)	$^{2}PDFGH$ (2) ^{4}PF	$^{2,4}F \rightarrow {}^{2,4}DFG$
9 (Cu^{2+}, Zn^{3+})	$^{1,3}D$	^{1}PDF ^{3}PDF	^{1}SDG ^{3}PF	$^{1,3}D \rightarrow {}^{1,3}PDF$

[a] High-spin multiplets stemming from the d^{n-1} electron configuration are not of direct relevance for the Kβ emission profile, but because of their interactions with the core ionized states they were taken into account; the small numerals under the term designation show the number of terms of the kind occurring in the configuration.

Numerical values for energies (ΔE) and oscillator strengths (f) of transitions of relevance for Kβ mainline XES for selected free 3d ions showing the dependence on charge and electronic configuration.

Table S5. Ti^{3+} (d^1)

	ΔE	f (x10^5)		ΔE	f (x10^5)
$^1D \rightarrow {}^1P$	0.00	32.05	$^3D \rightarrow {}^3P$	13.06	53.54
$^1D \rightarrow {}^1F$	12.85	74.94	$^3D \rightarrow {}^3F$	15.72	75.01
$^1D \rightarrow {}^1D$	13.07	53.55	$^3D \rightarrow {}^3D$	17.19	32.16

Table S6. V^{3+} (d^2)

	ΔE	f (x10^5)
$^2F \rightarrow {}^2D$	0.00	47.26
$^2F \rightarrow {}^2F$	6.03	48.18
$^2F \rightarrow {}^2G$	12.96	10.78
$^2F \rightarrow {}^2D$	13.60	4.66
$^2F \rightarrow {}^2F$	16.31	1.17
$^2F \rightarrow {}^2G$	16.40	107.82
$^2F \rightarrow {}^2F$	18.17	42.81
$^2F \rightarrow {}^2D$	18.37	13.83
$^4F \rightarrow {}^4D$	15.48	16.66
$^4F \rightarrow {}^4F$	18.63	92.29
$^4F \rightarrow {}^4G$	19.89	210.99
$^4F \rightarrow {}^4D$	21.97	49.28

Table S7. Cr^{3+}, Mn^{4+}, Fe^{5+} (d^3)

	$Cr^{3+}(d^3)$		$Mn^{4+}(d^3)$		$Fe^{5+}(d^3)$	
	ΔE	f (x10^5)	ΔE	f (x10^5)	ΔE	f (x10^5)
$^3F \rightarrow {}^3D$	0.00	40.16	0.00	42.57	0.00	44.91
$^3F \rightarrow {}^3F$	3.66	64.22	4.06	68.14	4.41	71.95
$^3F \rightarrow {}^3D$	6.21	4.74	6.76	5.01	7.21	5.26
$^3F \rightarrow {}^3D$	9.40	0.07	10.11	0.07	10.66	0.06
$^3F \rightarrow {}^3G$	10.49	26.48	11.57	27.75	12.51	28.93
$^3F \rightarrow {}^3F$	12.12	0.06	13.18	0.09	14.06	0.13
$^3F \rightarrow {}^3G$	15.33	0.14	16.87	0.26	18.20	0.40
$^3F \rightarrow {}^3F$	16.10	0.21	17.68	0.20	19.04	0.19
$^3F \rightarrow {}^3D$	16.63	7.05	18.35	7.56	19.84	8.06
$^3F \rightarrow {}^3G$	17.42	74.09	19.29	78.32	20.92	82.41
$^3F \rightarrow {}^3D$	18.37	0.03	20.29	0.04	21.97	0.04
$^3F \rightarrow {}^3F$	18.75	3.35	20.68	3.58	22.36	3.65
$^3F \rightarrow {}^3G$	20.73	21.15	22.94	23.44	24.88	25.64
$^3F \rightarrow {}^3D$	20.92	15.56	23.16	16.74	25.12	17.86
$^3F \rightarrow {}^3F$	21.29	26.83	23.59	28.77	25.61	30.66
$^5F \rightarrow {}^5D$	18.29	28.95	20.26	30.47	21.98	21.98
$^5F \rightarrow {}^5G$	22.22	121.99	24.70	129.89	26.89	26.89
$^5F \rightarrow {}^5F$	23.56	94.88	26.19	101.04	28.52	28.52
$^5F \rightarrow {}^5D$	24.34	38.81	27.05	41.69	29.43	29.43

Table S8. Cr^{2+}, Mn^{3+}, Fe^{4+} (d^4)

	$Cr^{2+}(d^4)$		$Mn^{3+}(d^4)$		$Fe^{4+}(d^4)$	
	ΔE	f (x10^5)	ΔE	f (x10^5)	ΔE	f (x10^5)
$^4D \rightarrow {}^4D$	0.00	66.33	0.00	70.15	0.00	73.97
$^4D \rightarrow {}^4P$	1.08	35.33	1.17	37.15	1.23	39.03
$^4D \rightarrow {}^4F$	6.29	65.04	7.07	68.14	7.72	71.33
$^4D \rightarrow {}^4D$	8.27	0.06	9.14	0.06	9.82	0.06
$^4D \rightarrow {}^4F$	10.72	0.98	11.90	1.30	12.80	1.64
$^4D \rightarrow {}^4P$	11.17	0.45	12.43	0.54	13.41	0.63
$^4D \rightarrow {}^4D$	11.42	0.36	12.74	0.37	13.79	0.38
$^4D \rightarrow {}^4F$	14.09	0.56	15.84	0.56	17.27	0.53
$^4D \rightarrow {}^4D$	15.50	0.25	17.36	0.23	18.88	0.32
$^4D \rightarrow {}^4D$	17.21	7.85	19.42	8.12	21.26	8.40
$^4D \rightarrow {}^4F$	17.25	51.15	19.49	54.10	21.38	57.02
$^4D \rightarrow {}^4P$	17.67	1.48	19.95	1.10	21.85	0.90
$^4D \rightarrow {}^4P$	18.17	17.56	20.51	19.33	22.46	20.91
$^4D \rightarrow {}^4F$	19.14	10.30	21.62	11.69	23.70	13.01
$^4D \rightarrow {}^4D$	19.90	16.50	22.49	17.88	24.67	19.26
$^6D \rightarrow {}^6P$	18.93	54.93	21.52	58.26	23.70	61.60
$^6D \rightarrow {}^6F$	20.47	125.19	23.28	135.98	25.65	143.74
$^6D \rightarrow {}^6D$	23.26	91.63	26.45	97.14	29.17	102.71

Table S9. Mn^{2+}, Fe^{3+}, Co^{4+} (d^5)

	$Mn^{2+}(d^5)$		$Fe^{3+}(d^5)$		$Co^{4+}(d^5)$	
	ΔE	f (x10^5)	ΔE	f (x10^5)	ΔE	f (x10^5)
$^5S \rightarrow {}^5P$	0.00	188.27	0.00	197.04	0.00	206.11
$^5S \rightarrow {}^5P$	13.71	3.50	15.22	3.63	16.49	3.73
$^5S \rightarrow {}^5P$	18.55	89.98	20.73	95.78	22.61	101.68
$^7S \rightarrow {}^7P$	22.01	282.41	24.77	297.31	27.18	312.26

Table S10. Fe^{2+}, Co^{3+} (d^6)

	$Fe^{2+}(d^6)$		$Co^{3+}(d^6)$	
	ΔE	f ($x10^5$)	ΔE	f ($x10^5$)
$^4D \rightarrow {}^4D$	0.00	67.64	0.00	70.17
$^4D \rightarrow {}^4F$	1.46	84.74	1.66	88.22
$^4D \rightarrow {}^4P$	4.58	31.60	5.11	32.83
$^4D \rightarrow {}^4D$	8.71	2.88	9.51	3.43
$^4D \rightarrow {}^4F$	9.47	1.42	10.34	1.46
$^4D \rightarrow {}^4D$	10.87	3.48	11.89	2.94
$^4D \rightarrow {}^4P$	11.92	1.38	13.15	1.41
$^4D \rightarrow {}^4D$	12.04	7.49	13.27	8.53
$^4D \rightarrow {}^4F$	12.63	2.91	13.97	3.06
$^4D \rightarrow {}^4P$	13.49	0.57	14.78	0.66
$^4D \rightarrow {}^4F$	17.09	2.93	18.89	3.09
$^4D \rightarrow {}^4D$	18.23	5.83	20.20	6.37
$^4D \rightarrow {}^4D$	19.13	8.70	21.20	9.03
$^4D \rightarrow {}^4F$	20.03	42.56	22.25	44.98
$^4D \rightarrow {}^4P$	21.32	24.17	23.71	25.50
$^6D \rightarrow {}^6P$	16.72	57.75	18.71	60.42
$^6D \rightarrow {}^6D$	21.97	96.32	24.52	100.80
$^6D \rightarrow {}^6F$	23.43	134.86	26.14	141.12

Table S11. Co^{2+}, Ni^{3+} (d^7)

	$Co^{2+}(d^7)$		$Ni^{3+}(d^7)$	
	ΔE	f (x10^5)	ΔE	f (x10^5)
$^3F\rightarrow{}^3D$	0.00	6.89	0.00	7.06
$^3F\rightarrow{}^3G$	3.80	80.30	4.31	83.21
$^3F\rightarrow{}^3F$	4.32	69.68	4.86	72.16
$^3F\rightarrow{}^3D$	7.22	23.40	8.00	23.68
$^3F\rightarrow{}^3F$	10.86	0.01	11.84	0.04
$^3F\rightarrow{}^3G$	10.98	6.64	12.16	7.08
$^3F\rightarrow{}^3D$	11.53	7.83	12.63	8.80
$^3F\rightarrow{}^3D$	12.36	4.18	13.60	4.24
$^3F\rightarrow{}^3F$	12.36	2.60	13.65	2.63
$^3F\rightarrow{}^3G$	14.68	0.19	16.14	0.17
$^3F\rightarrow{}^3D$	15.98	3.71	17.64	3.92
$^3F\rightarrow{}^3F$	17.07	4.54	18.79	4.84
$^3F\rightarrow{}^3G$	21.16	38.92	23.43	40.79
$^3F\rightarrow{}^3F$	21.58	21.27	23.92	22.36
$^3F\rightarrow{}^3D$	22.85	23.96	25.29	25.26
$^6F\rightarrow{}^6D$	15.92	61.03	17.75	63.36
$^6F\rightarrow{}^6F$	21.48	98.17	23.86	102.24
$^6F\rightarrow{}^6D$	21.95	9.06	24.29	9.66
$^6F\rightarrow{}^6G$	25.33	126.30	28.10	131.53

Table S12. Ni^{2+}, Cu^{3+} (d^8)

	$Ni^{2+}(d^8)$		$Cu^{3+}(d^8)$	
	ΔE	f (x10^5)	ΔE	f (x10^5)
$^2F\rightarrow{}^2D$	0.00	17.28	0.00	17.82
$^2F\rightarrow{}^2G$	1.61	91.99	1.82	95.07
$^2F\rightarrow{}^2F$	3.85	47.36	4.25	48.50
$^2F\rightarrow{}^2D$	7.39	33.70	8.13	34.82
$^2F\rightarrow{}^2F$	8.38	11.54	9.18	12.30
$^2F\rightarrow{}^2G$	15.01	36.23	16.46	37.90
$^2F\rightarrow{}^2D$	18.56	20.29	20.37	21.25
$^2F\rightarrow{}^2F$	19.23	40.95	21.11	42.72
$^4F\rightarrow{}^4D$	11.73	55.72	12.95	57.39
$^4F\rightarrow{}^4F$	15.32	99.87	16.89	103.56
$^4F\rightarrow{}^4D$	16.85	15.58	18.49	16.54
$^4F\rightarrow{}^4G$	21.24	128.49	23.36	133.26

Table S13. $Cu^{2+}(d^9)$

	$Cu^{2+}(d^9)$	
	ΔE	f ($x10^5$)
$^1D \rightarrow {}^1F$	0.00	141.65
$^1D \rightarrow {}^1P$	1.23	60.69
$^1D \rightarrow {}^1D$	13.44	101.43
$^3D \rightarrow {}^3D$	8.20	101.31
$^3D \rightarrow {}^3P$	9.04	60.80
$^3D \rightarrow {}^3F$	14.33	141.92

Table S14. $Fe^{1+}(3d^64s^1)$

	$Fe^{1+}(3d^64s^1)$	
	ΔE	f ($x10^5$)
$^5D \rightarrow {}^5D$	0.00	58.90
$^5D \rightarrow {}^5F$	5.08	95.49
$^5D \rightarrow {}^5D$	5.54	8.57
$^5D \rightarrow {}^5F$	8.63	123.17
$^7D \rightarrow {}^7P$	10.16	57.45
$^7D \rightarrow {}^7D$	15.26	95.91
$^7D \rightarrow {}^7F$	16.68	134.12

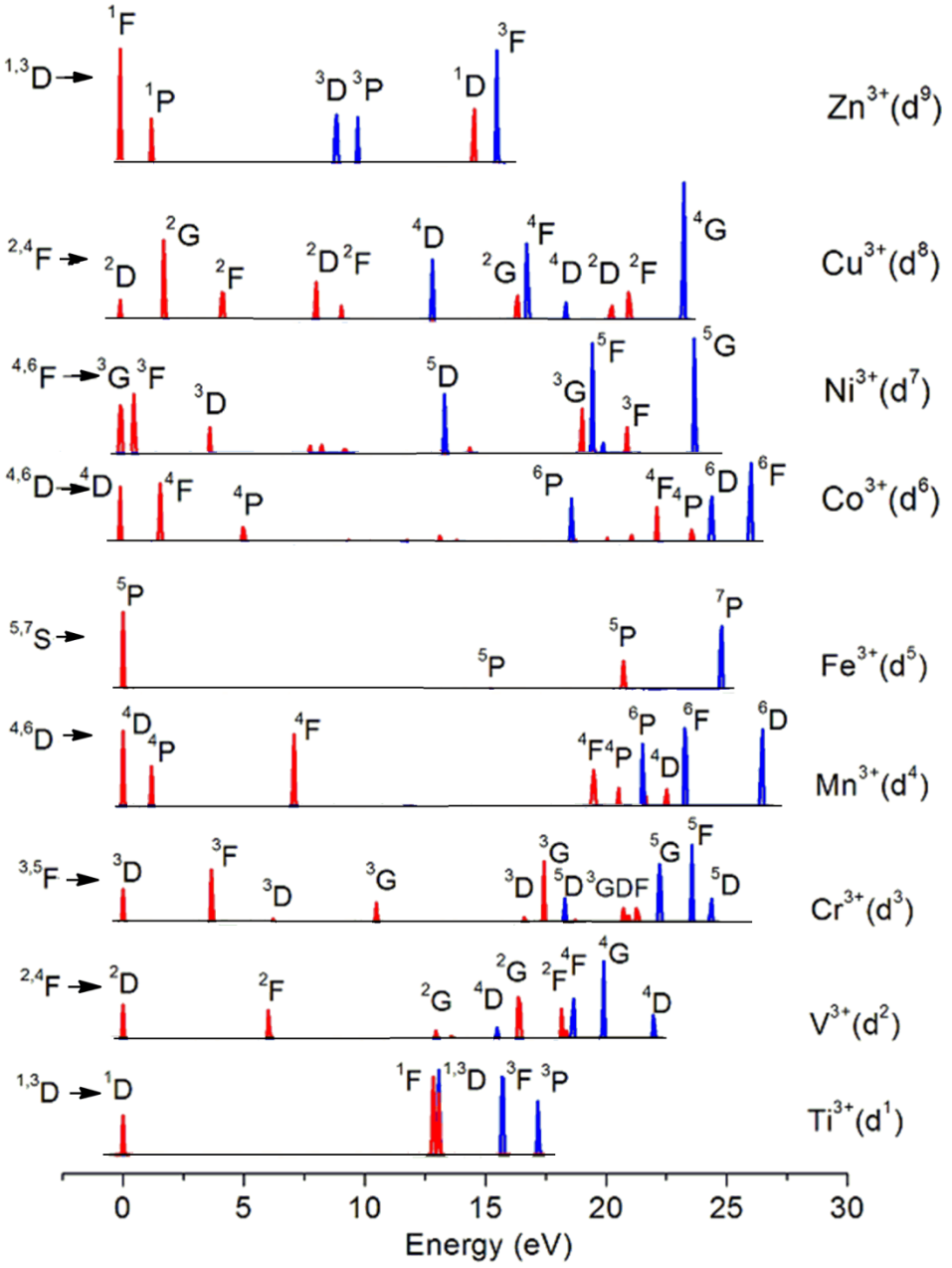

Figure S8. Theoretical non-relativistic CASSCF/RAS-CI spectra of M^{3+} transition metal ions showing dependence on the d^n configuration (spin-state) of the 3d-metal. Blue and red emission lines refer to ferro- and antiferromagnetic coupling of the spin of the core hole in the initial $1s^1$ and final $3p^5$ state with the entire manifold of the d^n mutliplets. Numerical values for the energies and oscillator strengths are listed in Tables S5-S14. Spectra have been plotted employing an artificially small line broadening (half-width-at-half maximum) of 500 cm^{-1} in order to allow the identification of individual multiplets. Intensities are in arbitrary units but otherwise comparable between the given ions.

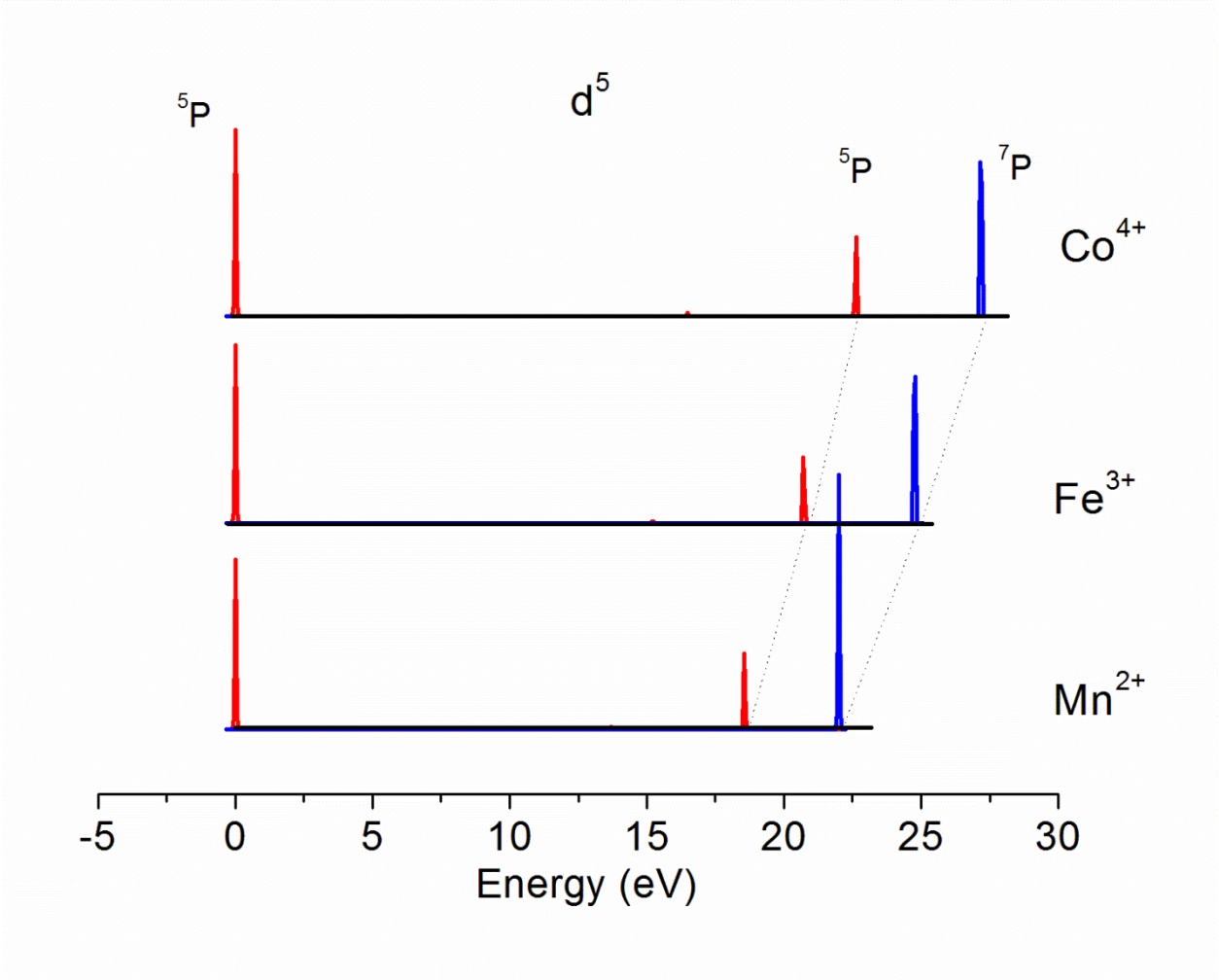

Figure S9. Dependence of the splitting of the Kβ mainline spectrum on the charge of isoelectronic (d^5) 3d ions from CASSCF/RAS-CI calculations (see Table S9 for numerical values of transition energies and oscillator strengths). Spectra have been plotted employing a line broadening (half-width-at-half maximum) of 500 cm^{-1}.

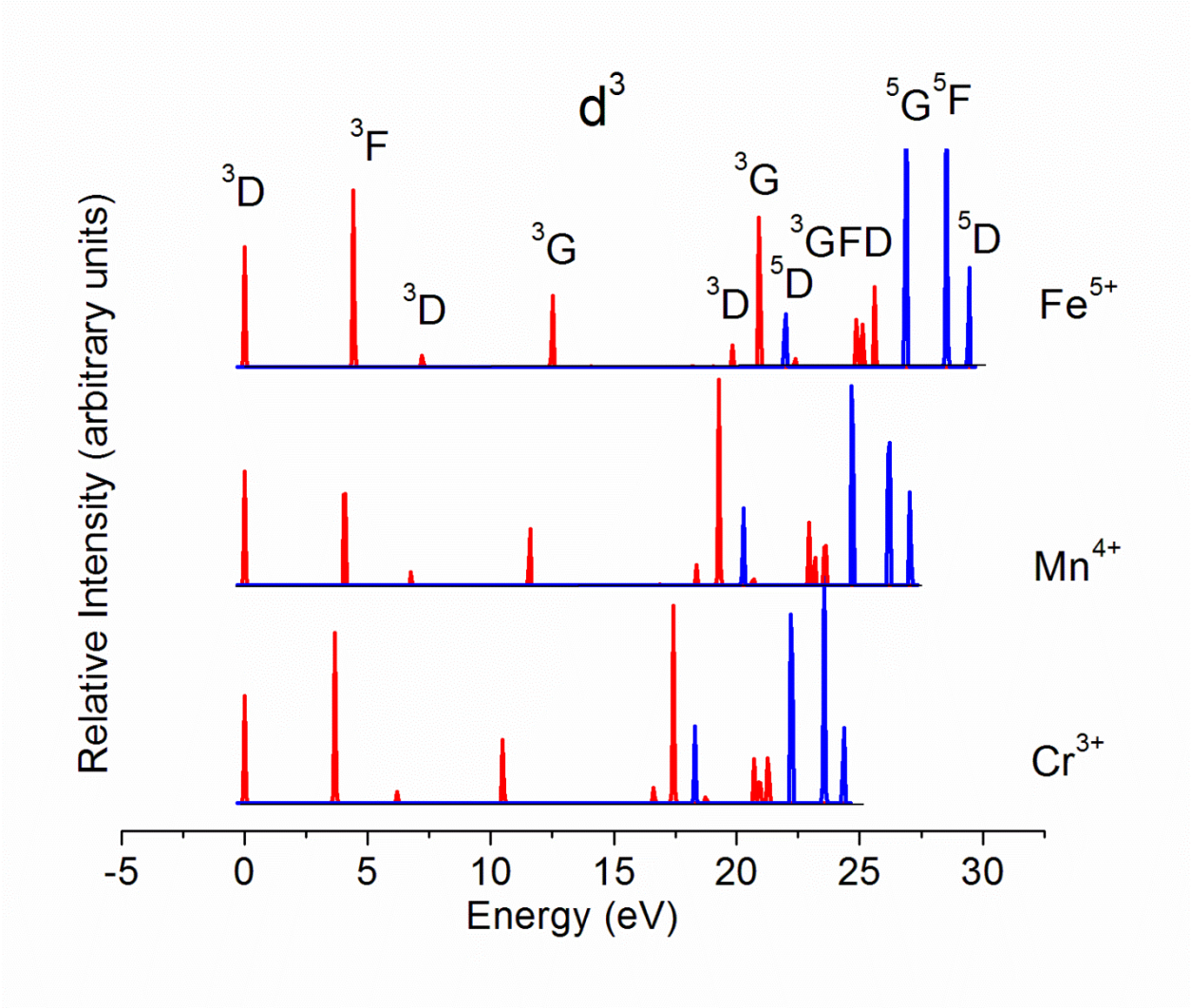

Figure S10. Dependence of the splitting of the Kβ mainline spectrum on the charge of iso electronic (d^5) 3d ions from CASSCF/RAS-CI calculations (see Table 5 for numerical values of transition energies and oscillator strengths). Spectra have been plotted employing a line broadening (half-width-at-half maximum) of 500 cm^{-1}.

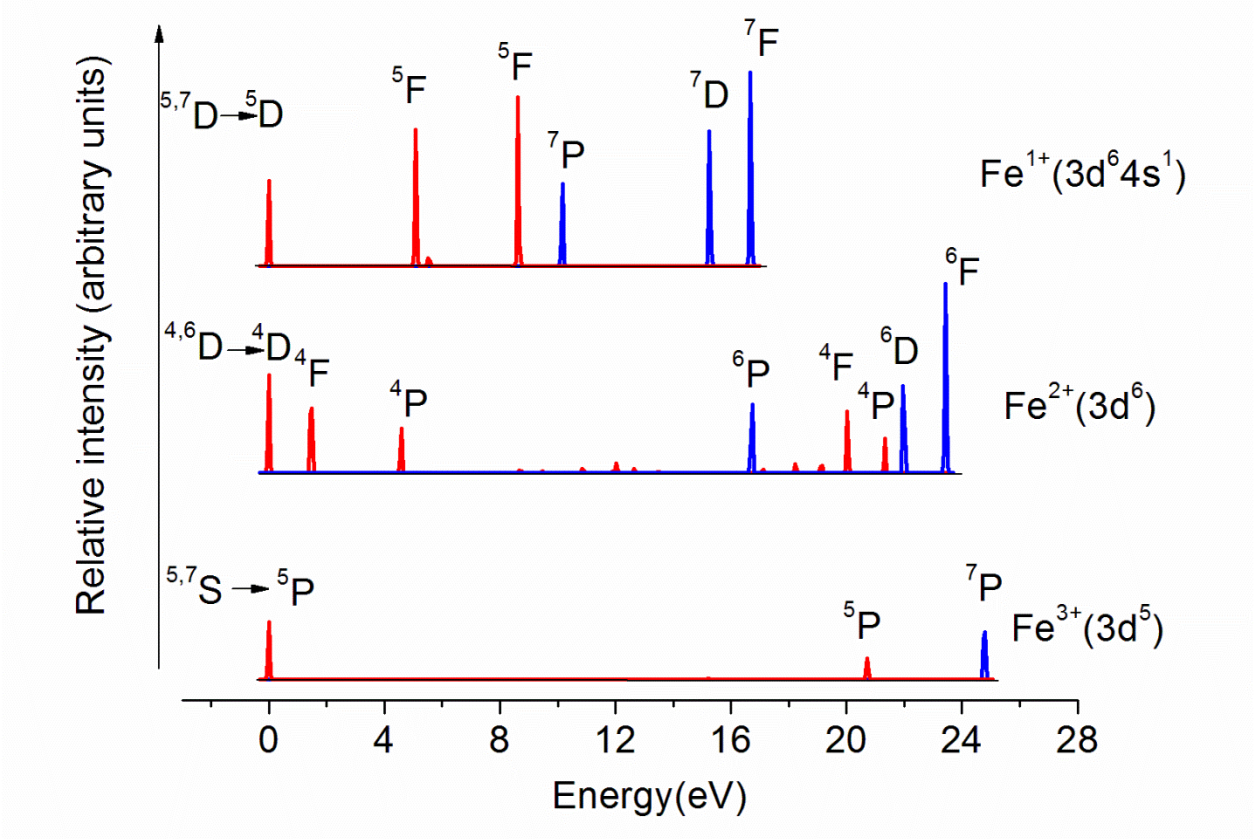

Figure S11. Theoretical CASSCF/RAS-CI Kβ mainline spectra of the Fe^{3+}, Fe^{2+} and Fe^{1+} free ions. Notice the that the ground state electronic configuration for Fe^{1+} is $3d^64s^1$, not $3d^7$; see Table S9, S10 and S11 for numerical values of transition energies and oscillator strengths for Fe^{3+}, Fe^{2+} and Fe^{1+}, respectively). Spectra have been plotted employing a line broadening (half-with-at-half maximum) of 500 cm^{-1}.

13 Slater-Condon and 3p-3d Exchange Coupling Parameters for Free 3d-Transition Metal Ions from Calculations at the Hartree-Fock Limit.

Values of Slater-Condon parameters G^1_{pd}, G^3_{pd} and $4G_1 + 42G_3$ (in eV) are included in the Tables **S15** and Table **S16**, respectively.

Table S15. Values (in eV) of G_1 (G_3).[a]

d-count	Cr	Mn	Fe	Co
2	16.036 (9.946)	-	-	-
3	15.381 (9.452)	16.793 (10.407)	-	-
4	14.603 (8.890)	16.149 (9.922)	17.547 (10.866)	-
5	-	15.395 (9.376)	16.912 (10.388)	18.296 (11.322)
6	-	-	16.176 (9.854)	17.670 (10.851)
7	-	-	-	16.949 (10.328)

[a] From calculations using Hartree-Fock self-consistent field theory (program by R.D.Cowan, 1981, "The Theory of Atomic Structure and Spectra", U.California Press, Berkeley); $G_1 = G^1_{pd}/15$; $G_3 = G^3_{pd}/245$.

Table S16. The 3p-3d exchange energy (per spin pair) $4G_1 + 42G_3$ (in eV).

d-count	Cr	Mn	Fe	Co
2	7.025	-	-	-
3	6.738	7.357	-	-
4	6.398	7.075	7.678	-
5	-	6.744	7.409	8.015
6	-	-	7.087	7.741
7	-	-	-	7.425

References

1. de Groot, F. M. F.; Fuggle, J. C.; Thole, B. T.; Sawatzky, G. A., *Phys Rev B* **1990,** *42*, 5459-5468.
2. Neese, F., *J. Chem. Phys.* **2005,** *122*, 034107-13.
3. Ganyushin, D.; Neese, F., *J. Chem. Phys.* **2006,** *125*, 024103-11.
4. McWeeny, R., *Methods of Molecular Quantum Mechanics*; Academic Press: London, 1992.